Intersubband hole-phonon and alloy disorder scattering in SiGe quantum wells

Z. Ikonić,* P. Harrison, and R. W. Kelsall
Institute of Microwaves and Photonics, School of Electronic and Electrical Engineering, University of Leeds, Leeds LS2 9JT, United Kingdom

(Received 10 May 2001; revised manuscript received 13 August 2001; published 29 November 2001)

Using the 6×6 $\mathbf{k}\cdot\mathbf{p}$ method we calculate hole-phonon and alloy disorder scattering rates in SiGe quantum wells, and how these depend on the various parameters of the system. The relative importance of different branches of nonpolar optical and acoustic phonons is discussed, and a comparison is made with alloy scattering. The latter is found to be an important mechanism for intersubband hole relaxation, particularly for low-energy transitions at low temperatures, where it dominates over phonon scattering, while losing significance in the opposite case. The results are relevant for the design and operation of SiGe-based quantum cascade lasers relying on intersubband transitions in the valence band.

DOI: 10.1103/PhysRevB.64.245311 PACS number(s): 73.21.Fg

I. INTRODUCTION

P-type Si/SiGe heterostructures are presently being considered as prospective candidates for intersubband (quantum cascade) lasers operating in a range of wavelengths, from midinfrared or even near infrared[1–3] to far-infrared[4]. Possible advantages offered by the *p*-Si/SiGe system include those of fundamental character (no polar optical phonons, in contrast to the $Al_xGa_{1-x}As$ and $Ga_xIn_{1-x}As/Al_yIn_{1-y}As$ systems, and a large nonpolar optical phonon energy in Si, which should result in increased relaxation times), as well as those of technological character (both in-plane and perpendicular polarizations of light are optically active, offering the prospect of surface-emitting intersubband lasers, and also low cost processing and the potential for integration).

Very important issues for intersubband laser operation are carrier relaxation rates, since these determine the achievable gain, the dynamics of the system, and the eventual modulation limits. In this paper we consider the relaxation processes between hole subbands in *p*-doped SiGe-based quantum wells (QW's) induced by phonon and alloy disorder scattering. The hole subband structure is calculated using the 6×6 $\mathbf{k}\cdot\mathbf{p}$ method. In the scattering calculations we do not use the axial approximation or the parabolic dispersion approximation; rather the full anisotropy of the quantized hole states is accounted for.

II. THEORY

A. Hole subband structure

Using basis set and state ordering as in Ref. 5, the block-diagonalized form of the 6×6 Hamiltonian [which includes heavy-hole (HH), light-hole, and split-off (SO) bands] reads

$$H=\begin{bmatrix} H_+ & 0 \\ 0 & H_- \end{bmatrix}, \tag{1}$$

where

$$H_\pm = \begin{bmatrix} P+Q & R\mp iS & \sqrt{2}R\pm\frac{i}{\sqrt{2}}S \\ R\pm iS^\dagger & P-Q\mp iC & \sqrt{2}Q\mp i\sqrt{3/2}\Sigma \\ \sqrt{2}R\mp\frac{i}{\sqrt{2}}S^\dagger & \sqrt{2}Q\pm i\sqrt{3/2}\Sigma^\dagger & P+\Delta\pm iC \end{bmatrix}, \tag{2}$$

and

$$P=\left(\frac{\hbar^2}{2m_0}\right)[\gamma_1(k_x^2+k_y^2)+k_z\gamma_1k_z],$$

$$Q=\left(\frac{\hbar^2}{2m_0}\right)[\gamma_2(k_x^2+k_y^2)-2k_z\gamma_2k_z],$$

$$R=\sqrt{3}\left(\frac{\hbar^2}{2m_0}\right)\gamma_\phi k_{||}^2,$$

$$S=2\sqrt{3}\left(\frac{\hbar^2}{2m_0}\right)k_{||}[(\sigma-\delta)k_z+k_z\pi],$$

$$\Sigma=2\sqrt{3}\left(\frac{\hbar^2}{2m_0}\right)k_{||}\left\{\left[\frac{1}{3}(\sigma-\delta)+\frac{2}{3}\pi\right]k_z + k_z\left[\frac{2}{3}(\sigma-\delta)+\frac{1}{3}\pi\right]\right\},$$

$$C=2\left(\frac{\hbar^2}{2m_0}\right)k_{||}[k_z(\sigma-\delta-\pi)-(\sigma-\delta-\pi)k_z],$$

$$\gamma_\phi=\sqrt{\overline{\gamma}^2+\mu^2-2\overline{\gamma}\mu\cos\phi}.$$

Here $\gamma_{1,2,3}$ are the Luttinger parameters, and their linear combinations, introduced by Foreman[5], are given by $\overline{\gamma}=(\gamma_3+\gamma_2)/2$, $\mu=(\gamma_3-\gamma_2)/2$, $\delta=(1+\gamma_1+\gamma_2-3\gamma_3)/9$, $\sigma=\overline{\gamma}-\delta/2$, and $\pi=\mu+3\delta/2$. The energy is measured from the valence band (VB) top downward, $k_{||}^2=k_x^2+k_y^2$, and

$\tan(\phi)=k_y/k_x$. This Hamiltonian does not include the axial approximation. In a one-dimensional-modulated, i.e., layered structure $k_z \rightarrow -i\partial/\partial z$, the quantities $\gamma_{1,2,3}$, μ, $\overline{\gamma}$, σ, δ, and π all vary along the z axis, and the position-dependent VB edge is added to the diagonal terms. This may include the valence-band offset, the external field bias, and, if the calculation is self-consistent, the self-consistent potential as well. Furthermore, in [001]-grown SiGe structures there exists a biaxial strain, i.e., $\epsilon_{xx}=\epsilon_{yy}\neq\epsilon_{zz}$ and $\epsilon_{xy}=\epsilon_{yz}=\epsilon_{zx}=0$, where the strain components amount to $\epsilon_{xx}=\epsilon_{yy}=(a_0-a_{lat})/a_{lat}$ and $\epsilon_{zz}=-(2C_{12}/C_{11})\epsilon_{xx}$, with a_{lat} denoting the lattice constant of the substrate (and hence the in-plane lattice constant of each layer), and a_0 the unstrained lattice constant of a particular layer. The P and Q terms are then amended with strain-dependent terms, i.e., $P \rightarrow P+P_\epsilon$, where $P_\epsilon=-a_v(\epsilon_{xx}+\epsilon_{yy}+\epsilon_{zz})$, and $Q \rightarrow Q+Q_\epsilon$, where $Q_\epsilon=-b(\epsilon_{xx}+\epsilon_{yy}-2\epsilon_{zz})/2$, where a_v and b are the hydrostatic and shear deformation potentials.

The eigenproblem to be solved,

$$H_{\pm}\Psi_{\pm}=E\Psi_{\pm}, \quad \Psi_{\pm}(\vec{r})=\psi_{\pm}(z)\exp[i(k_x x+k_y y)], \tag{3}$$

where $\psi_+(z)=[F_1(z)F_2(z)F_3(z)]^T$ and $\psi_-(z)=[F_4(z)F_5(z)F_6(z)]^T$, is further handled by expanding the wave functions in Fourier series,

$$F_j(z)=\sum_l F_j^{(l)} \exp(ig_l z), \quad g_l=l\frac{2\pi}{L} \tag{4}$$

where L is the periodic length of the structure (which, because of the solution method, is implicitly assumed to be a superlattice). A finite number N_z of g_l vectors is taken. For each wave-function basis component $F_i(z)$, there is a vector of Fourier components, which collectively comprise the Fourier representation of the total wave function.

The use of the Fourier expansion method was first proposed in Ref. 6, and was also used more recently,[7–9] though apparently not with Foreman's formulation of the Hamiltonian with the position-dependent Luttinger parameters. Here we describe briefly how the matrix elements are set up in this case.

Each of the terms in Hamiltonian (2), when acting upon a wave function, has one of the following four forms: (i) $f(z)\psi(z)$, (ii) $(d/dz)[f(z)\psi(z)]$, (iii) $f(z)(d/dz)\psi(z)$, and (iv) $(d/dz)[f(z)(d/dz)\psi(z)]$, where $f(z)$ represents a particular combination of Luttinger parameters and/or the potential, with appropriate constants [i.e., these $f(z)$'s are known functions at the time of setting up the Hamiltonian]. All the more complex derivatives, when they appear, are then expanded to obtain simple derivatives of the wave function, multiplied by another *known* function, or its derivative; i.e., $(d/dz)[f(z)\psi(z)] \rightarrow (df/dz)\psi+f(d\psi/dz)$, and $(d/dz)[f(z)(d/dz)\psi(z)] \rightarrow (df/dz)(d\psi/dz)+f(d^2\psi/dz^2)$.

To set up the Hamiltonian in the Fourier representation, the Fourier transforms of all the position-dependent quantities appearing in the Hamiltonian (the Luttinger parameters, and the potentials) are calculated. Then, using the fact that, if the lth Fourier component of $y(z)$ is $y^{(l)}$ then the lth component of $dy(z)/dz$ is $ig_l y^{(l)}$, we proceed in the conventional way, i.e., by substituting the Fourier expansion [Eq. (4)] of the wave function into the Schrödinger equation, left multiplying it by any one conjugate harmonic, integrating, and then using the orthogonality of plane waves. Thus we find that a matrix element (l,j) of the Hamiltonian, stemming from the operator $f(z)d^2/dz^2$, reads $f^{(k)}(ig_j)^2$; that from the operator $(df/dz)d/dz$ reads $(ig_k)f^{(k)}(ig_j)$, and that from the potential-like operator $f(z)$ is just $f^{(k)}$, where k is the subscript of the plane wave $g_k=g_l-g_j$ (if any such g_k lies outside the range included, then the matrix element is equal to zero). The method can be generalized straightforwardly to handle structures modulated in more than one direction, e.g., for quantum wires and dots.

B. Phonon scattering

The absence of polar-optical-phonon scattering in SiGe means that the two types of phonons relevant for hole scattering are the acoustic and nonpolar optical modes. The phonon branch dispersions, and the deformation potentials for hole-phonon scattering in pure Si and Ge, have been well documented. The situation in SiGe alloys is more complicated, due to considerable differences in some phonon properties in Si and Ge. For optical phonons the alloy has three distinct branches, corresponding to Ge-Ge, Ge-Si, and Si-Si interatomic vibrations. Each of them has it own distinct frequency and scattering deformation potential (that of Ge-Si is approximately the average of Ge-Ge and Si-Si branches). Separate branches are given appropriate strengths, according to the number of interatomic bonds present in the alloy. Thus, for an alloy with a Ge mole fraction x, these strengths amount to x^2, $2x(1-x)$, and $(1-x)^2$ for the Ge-Ge, Ge-Si, and Si-Si branches, respectively[10]. This concept, however, is not used for acoustic phonons with their comparatively small energies, and weighted averages of the velocities and of the deformation potentials of Si and Ge are usually taken.

Most of papers published so far on hole-phonon scattering dealt with bulk, or bulklike material (i.e., with no quantized hole states).[11–18] Various approaches to calculating the hole-phonon scattering rates have been used, from assuming a fully isotropic phonon dispersion, and a simple structure of the valence-band states, to including the anisotropy and complex structure of both carriers and phonons. The hole-phonon scattering in Si or SiGe QW's was studied in a limited number of papers.[10,19–22] In QW structures the phonons may be modeled as bulklike or confined. The Monte Carlo simulation in Ref. 21 assumed a parabolic dispersion and bulklike phonons, while the calculations presented in Refs. 10, 19, and 20 used confined phonons but the hole dispersion was taken as parabolic (the last two references dealt with heavy-hole subbands only, assuming parabolic subband dispersions and no mixing of heavy- and light-hole states). In a recent calculation[22] of scattering between LH and HH subbands, in which only acoustic phonons were considered, nonparabolicity was partly taken into account. More precisely, the dispersion of the LH1 state was modeled by a nonparabolic (i.e., shifted-parabolic) expression, to fit the $\mathbf{k}\cdot\mathbf{p}$ calculation, while the lower HH1 state was considered parabolic, and the

anisotropy of both states was neglected (this is a good approximation for the LH1 state, but not as good for the HH1 state). Furthermore, the basis overlap of quantized states was modeled by an independent simple expression after Wiley,[23] although the nonparabolicity, the anisotropy, and the wave-function overlap properties all originate from a common source, i.e., from the HH-LH-(SO) state mixing.

In this work we have used fully anisotropic hole subband dispersions, and full wave functions as calculated from the 6×6 $\mathbf{k}\cdot\mathbf{p}$ method, rather than using the Wiley factor. For phonons, however, we have adopted the model of bulklike phonons with isotropic dispersion.

The hole scattering rate from a quantized state i to state f due to acoustic phonon absorption and emission was calculated from[24]

$$W_{if}(\mathbf{k}_{||i}) = \frac{D_A^2 \hbar}{2\rho(2\pi)^2} \int_{(\mathbf{K})} \left(N_{ph} + \frac{1}{2} \pm \frac{1}{2} \right) |G_{if}|^2 \times \frac{K^2}{\hbar\omega_{ph}} \delta(E_i - E_f \pm \hbar\omega_{ph}) d\mathbf{K}, \tag{5}$$

and that due to nonpolar optical phonons from

$$W_{if}(\mathbf{k}_{||i}) = \frac{D_o^2 \hbar}{2\rho(2\pi)^2} \int_{(\mathbf{K})} \left(N_{ph} + \frac{1}{2} \pm \frac{1}{2} \right) |G_{if}|^2 \times \frac{1}{\hbar\omega_{ph}} \delta(E_i - E_f \pm \hbar\omega_{ph}) d\mathbf{K}, \tag{6}$$

where the integration in Eqs. (5) and (6) is performed over both the in-plane ($\mathbf{K}_{||}$) and the perpendicular (K_z) components of phonon wave vector $\mathbf{K}$, D_A and D_o are the acoustic- and optical-phonon deformation potentials, ρ is the material density, $\hbar\omega_{ph}$ is the phonon energy (which may depend on its wave vector), $N_{ph} = 1/[\exp(\hbar\omega_{ph}/k_B T) - 1]$, and

$$G_{if} = \int_{(z)} \psi^{\dagger}_{i,\mathbf{k}_{||i}}(z) \exp(iK_z z) \psi_{f,\mathbf{k}_{||f}}(z) dz \tag{7}$$

is the form factor for phonon scattering. The wave functions are vectors in the basis space, i.e., Eq. (7) accounts for both the spatial and basis overlaps of the initial and final states.

The wave functions in Eq. (7), and hence in Eqs. (5) and (6), depend on the in-plane wave vectors $\mathbf{k}_{||}$ of hole states (where $\mathbf{k}_{||f} = \mathbf{k}_{||i} \pm \mathbf{K}_{||}$), as does the energy, in an anisotropic and nonparabolic manner. There is, therefore, only a limited similarity between Eq. (7) and the corresponding quantity for electrons. The rates of various transitions will be determined by the interplay of $\mathbf{k}_{||}$-dependent state mixing and the oscillatory exponential effects in Eq. (7).

The above expressions give the ''bare'' scattering rates (i.e., assume empty final states), and also depend on the initial-state wave vector. More relevant quantity are the averaged scattering rates, which are obtained by inserting, into the integrals in Eqs. (5) and (6), the factor $[1 - f_{FD}(E_f(\mathbf{k}_{||f}), E_F, k_B T)]$, where f_{FD} is the Fermi-Dirac distribution function and E_F the Fermi level, and then forming averages according to[24] $\int f_{FD}(\mathbf{k}_{||i}) W_{if}(\mathbf{k}_{||i}) d\mathbf{k}_{||i} / \int f_{FD}(\mathbf{k}_{||i}) d\mathbf{k}_{||i}$. All the results presented in Sec. II C are for averaged scattering rates.

For the reasons described above, in contrast to the case of electron scattering, it is not possible to proceed with analytical integration in Eqs. (5) and (6), and further evaluation had to be done numerically. In the numerical procedure the hole-quantized state energies and wave functions were found at a number of points in the $\mathbf{k}_{||}$ plane, and a look-up table was made, to be used in a three-dimensional interpolation. The $\delta(\cdot)$ function was substituted with a Lorentzian whose width was determined according to the density of the numerical mesh used in the integration, and otherwise had no physical meaning. Since the procedure had to be numerical, there was no particular benefit to making the usual approximations about phonons (quasielastic scattering on acoustical phonons, dispersionless optical phonons), which are commonly employed in analytical considerations of electron-phonon scattering.

C. Alloy scattering

The alloy disorder scattering of electrons or holes was quite extensively considered in the literature, and included in transport studies of different types and levels of sophistication, in both bulklike[18,25–29] and quantized semiconductor structures.[30,31,21,35] In a random alloy of two elemental or binary compound semiconductors, e.g. with two constituents, with nominal (that is, the average taken over an infinite volume) contents of the constituents x and $1-x$, there occur fluctuations of the alloy composition when sampled in any finite volume. These fluctuations (alloy disorder) translate into an effective spatially fluctuating potential in the semiconductor, which gives rise to carrier scattering.

Interestingly, alloy scattering was almost exclusively studied in the context of carrier transport, in both SiGe and many III-V alloys, and it was found to be one of the major limiting mechanisms of carrier mobility, particularly at lower temperatures when phonon scattering is reduced. The alloy scattering is strictly elastic, and in bulklike semiconductors it is basically the direction of the carrier wave vector which is changed (although the wave-vector modulus may also change in the case of anisotropic dispersion). In quantized states of semiconductor nanostructures alloy scattering may, like all other types of scattering, be either intrasubband or intersubband, depending on whether the quantized state is conserved in scattering or not, such that in the former case it is just the in-plane wave vector $\mathbf{k}_{||}$ which is changed. For low-temperature carrier transport, almost all carriers reside in the lowest subband. Consequently, the transport properties are dominated by intrasubband scattering, and hence the intersubband processes have usually been neglected in theoretical studies of transport in HEMT's and other heterostructure devices.[31,21,35]

However, despite being elastic, alloy scattering can still contribute to carrier relaxation from excited subbands. In an intersubband alloy scattering process a carrier in a (typically) small-$k_{||}$ state, within an excited subband, will scatter into a larger-$k_{||}$ state of a lower (e.g., ground) subband, so that its total energy is conserved. From there, the carrier may cool,

i.e., lose energy by subsequent inelastic scattering involving acoustic or optical phonons. Intrasubband phonon scattering is generally a fast process, which makes it likely that a carrier will cool further before having a chance to scatter back into a higher subband. Therefore, alloy scattering may open an alternative carrier relaxation path in QW's. To the best of our knowledge, with the exception of the early study of Yoon *et al.*,[30] using simplified variational wave functions for conduction subbands for $Ga_yIn_{1-y}As$ based QW's, this mechanism has not attracted any further research attention.

It has been a common practice in alloy scattering calculations to model the scattering potential as a spherically symmetric square well of depth U_0 and radius r_0. There has been a degree of ambiguity of the actual definition of U_0 and, partly for this reason, a considerable spread of the reported values.[31] In fact, the alloy scattering potential is related to band-gap bowing in the alloy, another disorder-induced phenomenon, which may be calculated using the ionicity theory.[32] Since the band-gap bowing is an experimental quantity, it may provide a means of estimating the scattering potential in cases where it is not already known. Alternatively, one may choose a more intuitive approach, using the electron affinity or band discontinuity between the constituent materials.[33,34] The values thus obtained may help one obtain a good physical feeling, but to achieve a good quantitative agreement between the calculated scattering rates and experiment (carriers mobility) the alloy scattering potential is usually considered as an empirical or adjustable parameter.

The alloy scattering rate in a structure described by the composition profile $x(z)$, for transitions between the quantized states i and f with wave functions $\psi_{i,f}(z)$, is evaluated from[18,21,26,30,31]

$$W_{if}(\mathbf{k}_{||i}) = \frac{V}{(2\pi)^3}\frac{2\pi}{\hbar}\left(\frac{a_0^3}{4}U_0\right)^2\frac{N}{V^2}\cdot$$

$$\int_{(\mathbf{k}_{||})}|F(|\Delta k_{||}|)|^2 d\Delta\mathbf{k}_{||}\int_{(z)}x(z)\times[1-x(z)]\left|\psi^{\dagger}_{i,\mathbf{k}_{||i}}(z)\psi_{f,\mathbf{k}_{||f}}(z)\right|^2\times\delta[E_i(\mathbf{k}_{||i})-E_f(\mathbf{k}_{||i}+\Delta\mathbf{k}_{||})]dz, \quad (8)$$

where V is the volume of the system, $N=V/(a_0^3/4)$ is the total number of scatterers, each one having the (assigned) volume $a_0^3/4$, where a_0 is the lattice constant[26], $\Delta k_{||}=|\Delta\mathbf{k}_{||}|=|\mathbf{k}_{||i}-\mathbf{k}_{||f}|$ is the exchanged in-plane wave vector, and

$$F(\Delta k_{||}) = \frac{3\sin(\Delta k_{||}r_0)-3(\Delta k_{||}r_0)\cos(\Delta k_{||}r_0)}{(\Delta k_{||}r_0)^3} \quad (9)$$

is the form factor corresponding to the spherical well model, its radius r_0 being calculated from $4\pi r_0^3/3=a_0^3/4$.

While this single-primitive-cell sized scatterer model is usually employed, the above expression may be readily changed to handle the situation where there is prominent clustering in the alloy. Some degree of clustering may be expected purely on statistical grounds, and there may also be a strain-related tendency for it to appear during the course of epitaxial growth, even if it may not minimize the total energy of the already grown structure. If clustering does occur, one may assume that the size of an ''effective'' scatterer is equal to that of the clusters (though this clearly is a rather crude model, since there will still be some alloy disorder within clusters). With an average number N_c primitive cells in a cluster, Eq. (8) may be modified by the substitutions $a_0^3U_0/4\rightarrow N_c a_0^3U_0/4$ and $N\rightarrow N_c a_0^3/4$, and the scatterer radius in Eq. (9) is evaluated from $4\pi r_0^3/3=N_c a_0^3/4$. Mobility calculations using various-sized clusters were reported in the literature.[25]

A recently reported total-energy calculation for SiGe alloys,[36] with and without clustering, found no significant difference between the two. Hence no tendency toward clustering is expected, while clusters which occur statistically would be fully stable (and, with no thermodynamic preference for their formation, the majority of clusters would be very small). On the experimental side, clusters as large as 20–30 nm in SiGe/Si HEMT's were reported only when using pulse laser deposition,[37] but not in structures made by molecular-beam epitaxy (MBE) (in contrast, clustering in $In_xGa_{1-x}As$ and $In_yAl_{1-y}As$ normally appears in MBE as well[25,37]).

In the case of intrasubband scattering (e.g., for a calculation of the carriers mobility) one always uses the long-wavelength approximation ($\Delta k_{||}\ll 1/r_0$), effectively setting $F(\Delta k_{||})=1$ in Eq. (8). This is fully justified under near-equilibrium low-temperature conditions, because the initial state $k_{||i}$ is small and, even with anisotropy included, $\Delta k_{||}$ cannot much exceed $2k_{||i}$. Consequently, the value of the radius r_0 alone is irrelevant in this limit (i.e., one cannot tell whether there is any clustering present), because the alloy potential U_0 will eventually be determined by comparison with experiment (the quantity actually determined in this manner is the product $N_cU_0^2$).

The computational details are the same as those for phonon scattering, described above. To discuss the importance of various terms in Eq. (8) briefly, we note that for hole scattering in an intrasubband process both the spatial and the basis overlap are good, so scattering is very efficient. For intersubband scattering, however, the spatial overlap is clearly reduced, because any $|\psi|^2$ overlaps with itself better than it does with any other function, and the same is true for the basis overlap. However, this reduction is not too great, for two reasons. First, the spatial overlap involves the integral of an entirely positive function. Second, the hole states for large $k_{||}$ are highly mixed in character; hence there will be a substantial basis overlap of a near-zone-center state and a higher-$k_{||}$ state, whatever their character is at $k_{||}=0$. Concerning the overlap, therefore, intersubband scattering is expected to be smaller than intrasubband scattering, but will remain within an order of magnitude of the latter. Finally, the form factor [Eq. (9)] may additionally suppress intersubband scattering, depending on the magnitude of the exchanged wave vector relative to the inverse scatterer radius. $F(\Delta k_{||})$ will fall off with $\Delta k_{||}$ faster if the cluster size N_c is larger. The form factor influences the scaling of the scattering rate

with the energy difference between states (because this in turn defines the range of exchanged wave vectors), but only in conjunction with the basis- and spatial-overlap arguments.

III. NUMERICAL RESULTS AND DISCUSSION

Numerical calculations were performed for a range of SiGe/Si QW's of the conventional rectangular profile, with either $Ge_{0.3}Si_{0.7}$ or $Ge_{0.5}Si_{0.5}$ well layers, and Si barriers, while the substrate (which determines the strain conditions in the whole structure) was $Ge_{0.2}Si_{0.8}$. This choice of materials is appropriate for achieving strain-symmetrized structures, as a likely form of realization of multiple quantum wells intended for use in quantum cascade lasers. The relaxation rates are primarily determined by the well region, either directly (via its width and composition) or indirectly (via its strain conditions imposed by the substrate), because the wave functions are mostly localized in the wells, while the barriers have a much smaller influence (due to the wave functions repulsion into the well, and the absence of alloy disorder if made of pure Si). The Si and Ge parameters for the band structure calculations were taken from Ref. 38, except the VB offset which was set to the more realistic value $\Delta E_v = 0.56$ eV[39]. The parameters for the phonon scattering calculation were as in Ref. 21. The optical phonons were taken to be dispersionless, which is a reasonable approximation in view of the fact that phonons with K_z larger than $\sim 20\%$ of the extent of the Brillouin zone make no contribution to scattering, due to the oscillatory exponential in Eq. (7). Acoustic phonons were assumed to have a linear dispersion, which is adequate in the above range of wave vectors, and, as we discuss below, gives a noticeable difference from the results of the zero-energy acoustic-phonon model. The alloy scattering potential consistent with the scatterer size used here was $U_0 = 0.42$ eV.[31] In all the calculations the surface hole density was set at 5×10^{11} cm^{-2}.

In discussing the influence of various parameters on the scattering rates, it is useful to recall some properties of hole bound states in SiGe QW's. Once the well composition and the strain conditions (i.e., the substrate) are specified, the spacing between the HH1 state (always the lowest) and the LH1 state is almost independent of the well width for a wide range of values,[38] and in the above system amounts to ≈ 30 meV in the 30% Ge QW, and to ≈ 72 meV in the 50% Ge QW. In a range of well widths from 20 to 40 ML for instance, these LH1-HH1 spacings are stable to within 1 meV (where 1 ML is half the lattice constant, ≈ 2.8 Å for the [001] growth direction, as is conventional in SiGe QW's). On the other hand, the HH2-HH1 spacing depends mostly on the well width in the classical textbook manner, and widening the well makes the HH2 state swap position with LH1, to become the second lowest state. The HH2-HH1 spacing changes from ~ 80–90 meV down to ~ 25 meV in the above range of well widths. Therefore, the LH1-HH1 and HH2-HH1 spacings in the systems considered span an energy range which includes the characteristic values 37.3 meV (the Ge-Ge optical phonon energy) and 64.1 meV (the Si-Si optical phonon energy). Quantized states have pure HH or LH+SO character only at the zone center ($\mathbf{k}_{||} = 0$), and this is used for labeling the states, but they acquire progressively more mixed character as $k_{||}$ increases. In the case of almost adjacent (within a few meV) HH and LH states, the mixing is strong even for very small values of $k_{||}$. The inverted mass feature, which is considered useful for quantum cascade lasers,[4,22] also appears in this case.

Figure 1 shows the scattering rates from all the phonon branches, and the total rate, between the lowest three states in a 32-ML $Ge_{0.3}Si_{0.7}$ QW. The subband spacings in this well at $k_{||} = 0$ are $\Delta E_{LH1\text{-}HH1} = 31$ meV, $\Delta E_{HH2\text{-}HH1} = 38$ meV, and $\Delta E_{HH2\text{-}LH1} = 7$ meV, all of which are less than any of the three optical phonon energies, except $\Delta E_{HH2\text{-}HH1}$, which is only marginally larger than the Ge-Ge phonon energy. One can indeed see in Fig. 1(a), and even more so in Fig. 1(c), that the acoustic phonons are the most important relaxation routes for the LH1-HH1 and HH2-LH1 transitions in this structure. It is interesting to note that acoustical phonons are slightly more important even for the HH2-HH1 transition, even though it is almost ''resonant'' with the Ge-Ge optical phonon energy [Fig. 1(b)]. At low temperatures this is because only a small portion of the final $\mathbf{k}_{||}$ states are really accessible to holes which are populating only the $\mathbf{k}_{||} \approx 0$ initial states. At high temperatures, with holes populating a larger range of the initial $\mathbf{k}_{||}$ states, the absence of a strong ''resonant'' scattering with Ge-Ge optical phonons is due to the fact that HH1 and HH2 states, despite having the same character, have very different in-plane dispersions, due to mixing effects. Therefore, for the majority of holes the HH2-HH1 transition is not resonant with the Ge-Ge optical phonons at all. Indeed, a consequence of the band mixing is that the concept of resonantly enhanced optical phonon scattering is much less significant for hole intersubband transitions, compared to the case of electrons.

In another example we consider a 22-ML $Ge_{0.5}Si_{0.5}$ QW. The state spacings at $k_{||} = 0$ here are $\Delta E_{LH1\text{-}HH1} = 72$ meV, $\Delta E_{HH2\text{-}HH1} = 79$ meV, and $\Delta E_{HH2\text{-}LH1} = 7$ meV, the first two now being larger than all of optical phonon energies. The contributions of the optical phonons now exceed those of the acoustic phonons [Figs. 2(a) and 2(b)], except in the low-energy HH2-LH1 transition where the acoustic phonons are most important [Fig. 2(c)], as expected. What was not expected, however, and in contrast to the previous example, is that the HH2-HH1 optical phonon scattering rates do not show any significant increase with increasing temperature [Fig. 2(b)]. In fact, in the intermediate temperature range these rates *decrease* with temperature, though only slightly. This is actually a common feature we find in all cases where the HH2-HH1 spacing is large (significantly larger than the energy of the corresponding optical-phonon mode), hence the transitions are then necessarily highly skewed in k space. The phenomenon does not occur in analogous (''character-preserving'') scattering between the electronic subbands, indicating that it is the band mixing, present in hole systems, which brings about this unusual result. With increasing temperature the hole distribution spreads over a larger range of $k_{||}$ states of the HH2 subband, and the band-mixing effects then reduce the average overlap, i.e., the form factor (7). At the same time the phonon occupancy factor $N_{ph} + 1 = 1 + 1/[\exp(\hbar\omega_{ph}/k_B T) - 1]$ (because phonon emission predomi-

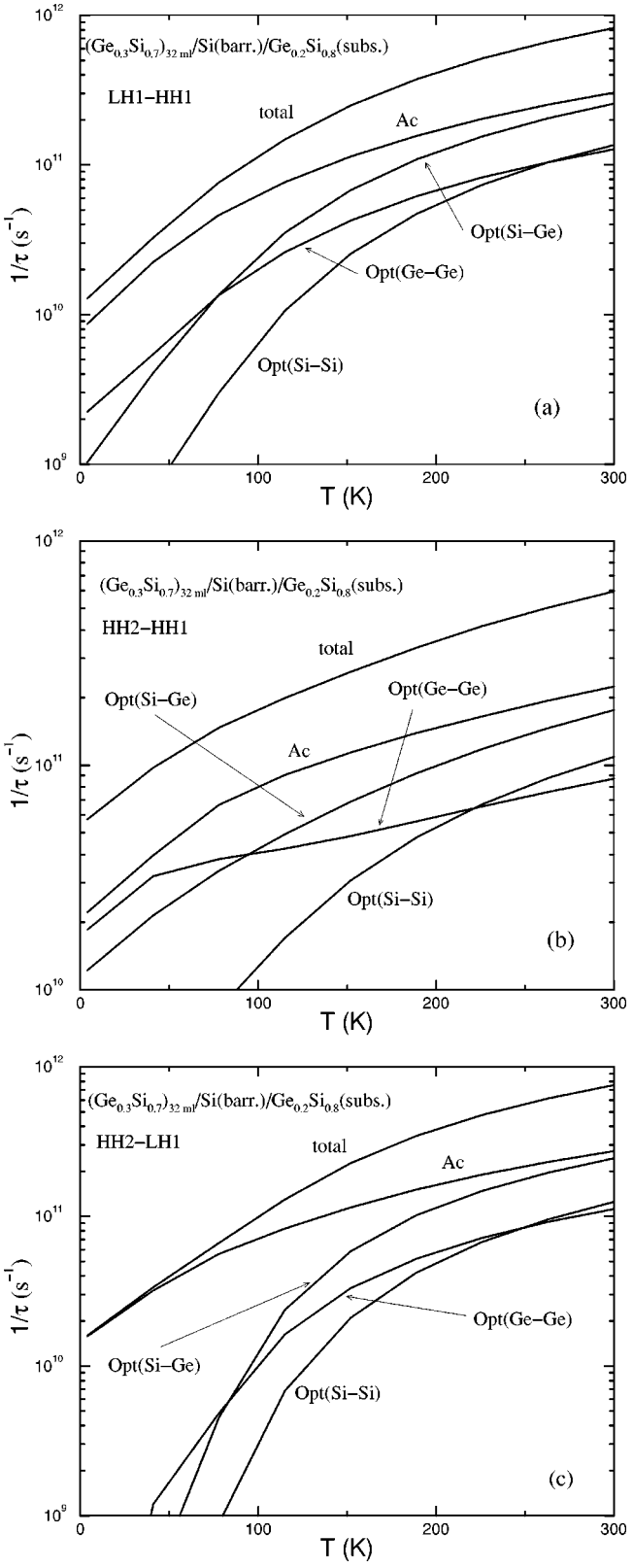

FIG. 1. The contributions of different phonon branches to the total intersubband scattering rates, as these depend on temperature, in a 32 ML (88.2 Å) wide $Ge_{0.3}Si_{0.7}$ QW, with Si barriers, and on the $Ge_{0.2}Si_{0.8}$ substrate, calculated for the (a) LH1-HH1, (b) HH2-HH1, and (c) HH2-LH1 transitions.

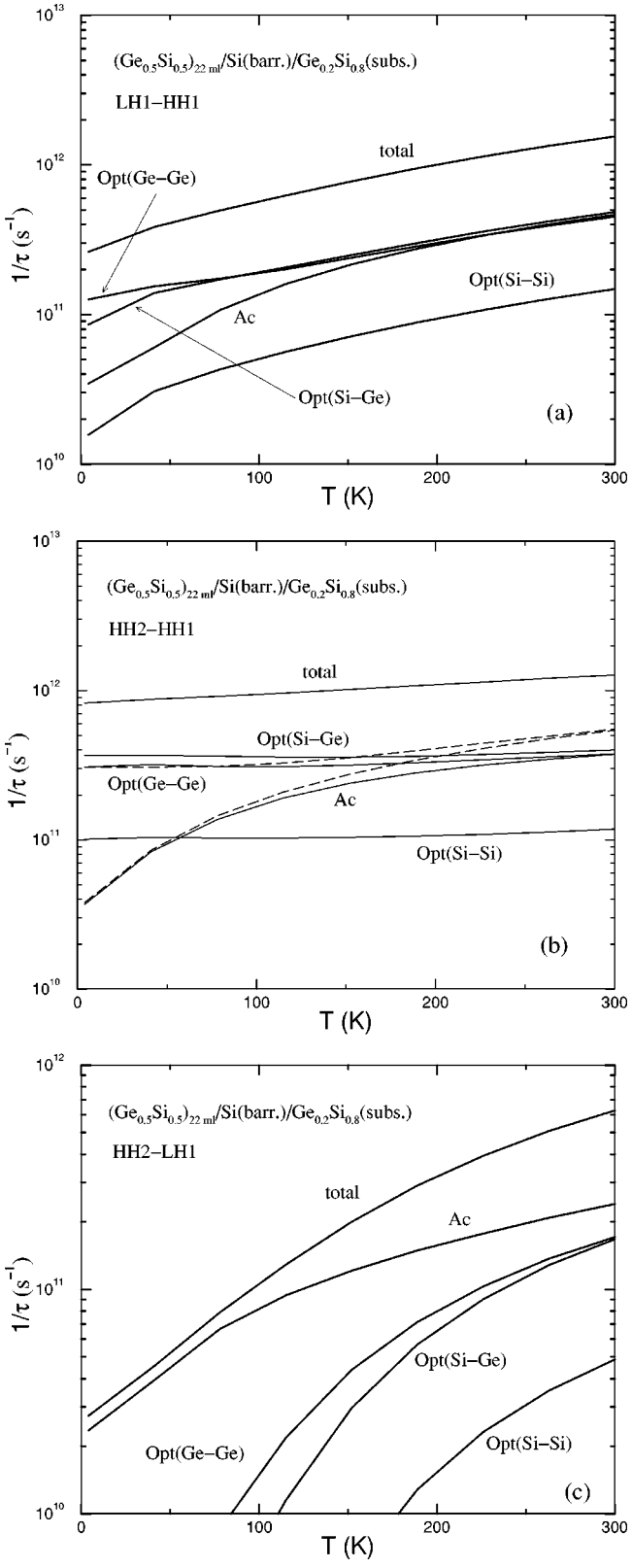

FIG. 2. Same as in Fig. 1, but for a 22 ML (60.6 Å) wide $Ge_{0.5}Si_{0.5}$ QW. The dashed lines in 2(b) represent the acoustic and Ge-Ge optical-phonon scattering rates calculated at $k_{||}=0$ only (without averaging over the initial states).

nates at these large state spacings) increases. For the optical modes this increase is rather mild ($\sim 33\%$ for temperatures below $T=300$ K for the Ge-Ge mode, even smaller for others), and is very large for the acoustic phonons with their smaller energies (but cannot be specified simply, due to their dispersive nature). The net effect is that the band-mixing and phonon occupancy are counterbalanced, and the averaged scattering rates on optical phonons depend only slightly on temperature. This is very prominent in the example given in Fig. 2(b), but the balance may be less perfect in other examples. On the other hand, the acoustic-phonon occupancy increases with temperature too strongly to be compensated for in this way, so the corresponding averaged scattering rate still increases. If the hole distribution and averaging were not accounted for, and only the scattering rates from the $k_{||}=0$ initial state were considered, one would obtain the more naturally looking but (in particular at high temperatures) incorrect result, also displayed in Fig. 2(b).

The dependence of the total phonon scattering rates on the well width, calculated at $T=77$ K, is given in Figs. 3(a) and 3(b). In both cases there is a rather slow variation of the LH1-HH1 rate, which is due to the fact that the spacing between these two states is almost independent of the well width. On the other hand, the HH2-HH1 scattering rate decreases with the well width, which may be ascribed to the fact that the HH2-HH1 spacing decreases, making one after another optical phonon type ineffective in scattering. The HH2-LH1 (or LH1-HH2, depending on the well width) relaxation rate also depends on the well width, and has a minimum approximately (but not exactly, probably due to the nonparabolicity and band mixing effects) where these two states cross at $k_{||}=0$. In the structures we have considered, this close proximity of the LH1 and HH2 states at $\mathbf{k}_{||}=0$ occurs for a 36-ML well with 30% Ge, or a 23-ML well with 50% Ge.

Figure 4 shows the influence of the quasielastic approximation for acoustic phonons (i.e., neglecting the phonon dispersion in the energy conservation condition, while retaining it in the phonon distribution function). In effect, forcing the scattering to be ''horizontal'' in the E-k space makes the final state for phonon emission more remote than it really is, and has the opposite effect in the case of phonon absorption. These errors apparently do not cancel out, but result in underestimating of form factor (7), reducing the calculated scattering rate by a factor of 1.5–2. We have also checked the possibility of using the axially isotropic in-plane dispersion of hole subbands in phonon scattering calculations, because it would clearly save a lot of computational effort. We have tried sampling the subband dispersions along various directions in the $\mathbf{k}_{||}$ plane (including that which is equivalent to using the axial approximation from the outset). This resulted in variations in the calculated scattering rates of up to one order of magnitude, and we could not find a single sampling direction which would be universal, and deliver the results of the anisotropic calculation. The importance of accounting for the anisotropy stems from the fact that it is quite strong in SiGe QW's, in particular for the ground HH1 state.

Next we present the results for the alloy scattering. Figure 5 shows the scattering rates between the lowest three states

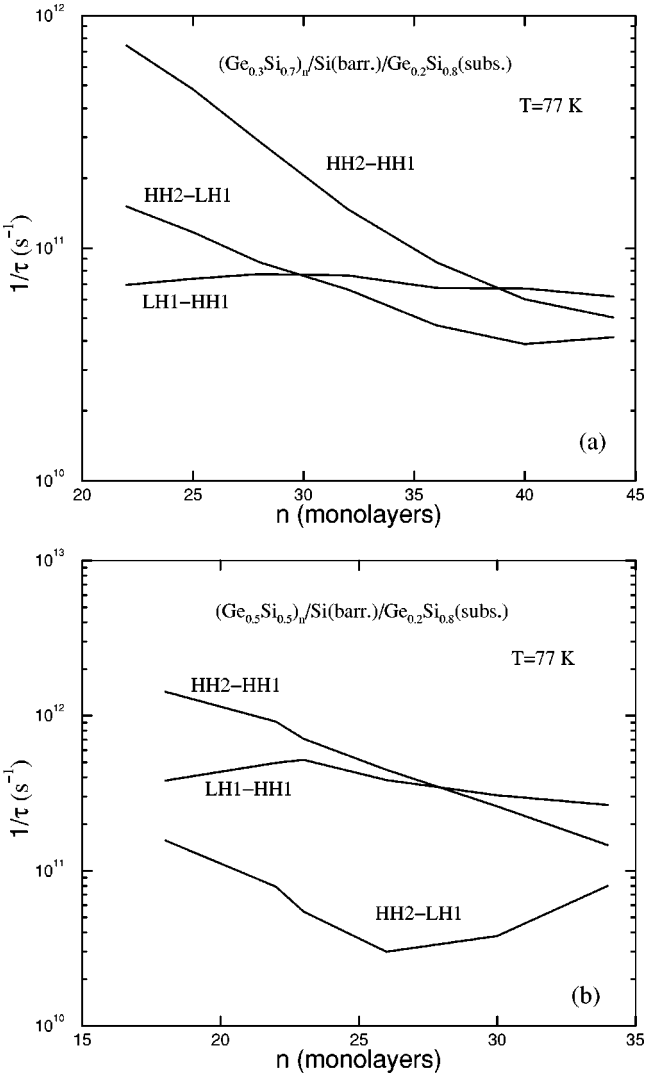

FIG. 3. The total hole-phonon intersubband scattering rates, as they depend on the well width, at $T=77$ K, in (a) $Ge_{0.3}Si_{0.7}$- and (b) $Ge_{0.5}Si_{0.5}$-based QW's.

in two QW's. The scattering rate between the like-character states (HH2-HH1) is more prominent for both QW's, but the mixed-character transitions are almost as strong, because a large exchanged $k_{||}$ vector implies that the composition of the final state will include a substantial proportion of the basis states which matches the initial state, as discussed above. For the same reason, and also due to the $x(1-x)$ term in Eq. (8), the scattering rates are larger in the thinner well with higher Ge content x, i.e., with larger energy spacings between the states. Although the microscopic scattering process is temperature independent (in contrast to hole-phonon scattering), the averaged rates shown in Fig. 5 depend slightly on temperature, because of the $k_{||}$-dependent state mixing taken together with the temperature dependence of the hole distribution over the $k_{||}$-states.

The influence of clustering (cluster size N_c) on the alloy scattering rates is given in Fig. 6. In this set of calculations, the value of the product $N_c U_0^2$ (and hence implicitly the hole mobility, as the experimentally measurable quantity) was

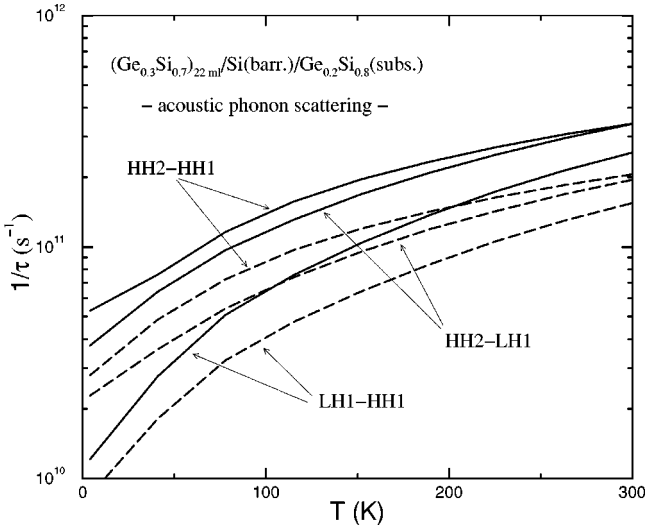

FIG. 4. The hole–acoustic-phonon intersubband scattering rates in 22-ML-wide $Ge_{0.3}Si_{0.7}$ QW calculated exactly (solid lines), and within the quasielastic scattering approximation (dashed lines).

kept constant. Under such conditions, in the range of transition energies of practical interest there is hardly any influence of the cluster size on intersubband relaxation for clusters of less than ~100 primitive cells, i.e., 200 atoms. Therefore, clustering in real MBE-grown samples (if it appears at all) probably has only a mild influence on the scattering rates.

The dependence of the alloy scattering rates on well width are shown in Fig. 7. There is clearly a general decrease of the scattering rates with well width, but only within a factor of ~2. The fact that alloy scattering rates are only weakly temperature dependent, while the phonon scattering rates generally have a stronger, and increasing, dependence on temperature, indicates that alloy scattering may be the principal relaxation mechanism in *p*-SiGe QW's with small ($\leqslant$30 meV) state spacings, at low temperatures. In such systems, important, e.g., for far-infrared (THz) quantum cascade lasers, alloy scattering may well be the limiting factor in the intersubband hole lifetimes.

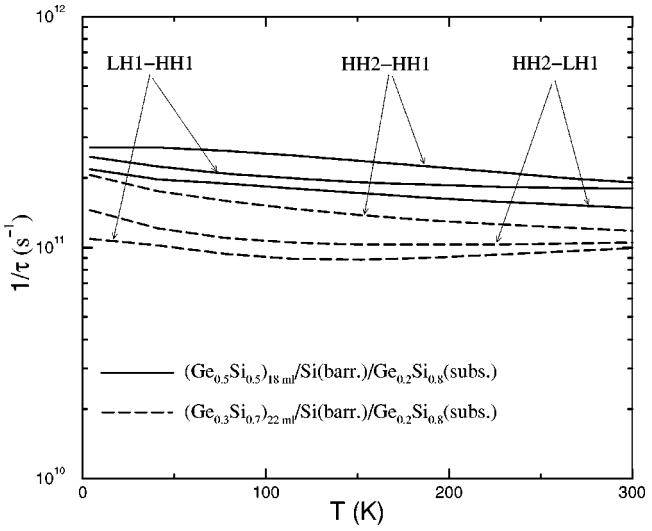

FIG. 5. The temperature dependence of the averaged alloy scattering rates between the lowest three hole quantized states (HH1, LH1, and HH2) in a 50.3 Å (18 ML) wide $Ge_{0.5}Si_{0.5}$ QW and a 60.6 Å (22 ML) wide $Ge_{0.3}Si_{0.7}$ QW, both with Si barriers, on a $Ge_{0.2}Si_{0.8}$ virtual substrate.

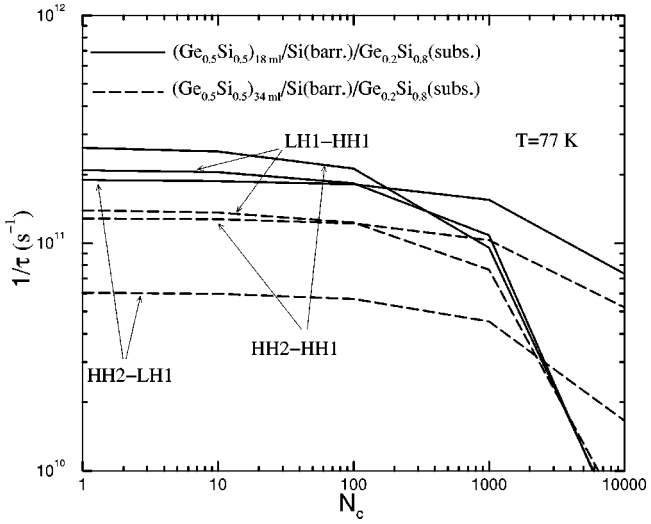

FIG. 6. The alloy scattering rates in the QW's described in Fig. 5, but calculated for a range of scattering cluster sizes, at $T = 77$ K.

IV. CONCLUSION

Calculations of the hole-phonon and alloy intersubband scattering rates in a range of SiGe QW's were performed. The hole subband structure was calculated using the 6×6 $\mathbf{k}\cdot\mathbf{p}$ method, and the full anisotropy of the in-plane dispersion of the quantized states was included. The relative importance of the different nonpolar optical phonons in the SiGe alloy layers, and of the acoustic phonons, was also

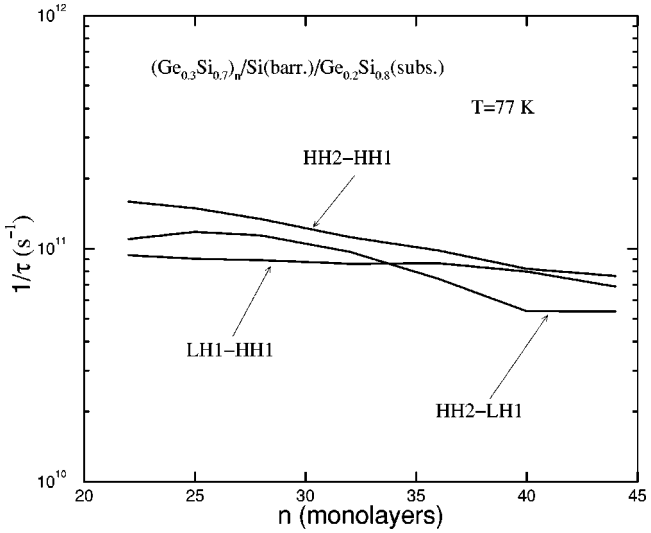

FIG. 7. The averaged alloy scattering rates vs the QW width calculated for $Ge_{0.3}Si_{0.7}$ QW's with Si barriers, on a $Ge_{0.2}Si_{0.8}$ virtual substrate, at $T = 77$ K.

discussed. For the low-energy transitions, which may be important for the operation of *p*-SiGe-based intersubband quantum cascade lasers, the acoustic phonons are the most important among phonon scattering mechanisms, but the optical phonons (in particular, the Ge-Ge mode) are also nonnegligible. However, for a range of *p*-SiGe QW's a very important mechanism for intersubband hole relaxation is the alloy scattering. Its relative importance is largest in case of small spacing between quantized states and at low temperatures, where phonon scattering is reduced, with typical lifetimes in the range of 3–10 ps, but it may remain important, though not dominant, in other cases as well. It should be noted that the importance of alloy scattering is rather specific to *p*-SiGe among the most common QW systems. This is because the confining (''well'') layers, in which most of the wave function is localized, are here made of alloy rather than of pure binary or elemental semiconductors, and there are no polar optical phonons. At least one of these properties is not shared with common GaAs/$Al_xGa_{1-x}As$ or $Ga_yIn_{1-y}As/Al_zIn_{1-z}As$ based QW's.

ACKNOWLEDGMENTS

This work is supported by DARPA/ USAF Contract No. F19628-99-C-0074. The authors thank W. Batty (Leeds) and R. A. Soref (Hanscom AFB) for useful discussions.

*Email address: z.ikonic@ee.leeds.ac.uk

[1] R. A. Soref, L. Friedman, and G. Sun, Superlattices Microstruct. **23**, 427 (1998).
[2] L. Friedman, R. A. Soref, G. Sun, and Y. Lu, IEEE J. Sel. Top. Quantum Electron. **4**, 1029 (1998).
[3] G. Dehlinger, L. Diehl, U. Gennser, H. Sigg, J. Faist, K. Ensslin, D. Grutzmacher, and E. Muller, Science **290**, 2277 (2000).
[4] L. Friedman, G. Sun, and R. A. Soref, Appl. Phys. Lett. **78**, 401 (2001).
[5] B. A. Foreman, Phys. Rev. B **48**, 4964 (1993).
[6] D. Gershoni, C. H. Henry, and G. A. Barraf, IEEE J. Quantum Electron. **29**, 2433 (1993).
[7] B. W. Kim, E. Mao, and A. Majerfeld, J. Appl. Phys. **81**, 1883 (1997).
[8] D. C. Hutchings, Superlattices Microstruct. **26**, 195 (1999).
[9] V. J. Hales, A. J. Poulter, and R. J. Nicholas, Physica E **7**, 84 (2000).
[10] K. Bhaumik, B. K. Ridley, and Y. Shacham-Diamand, J. Appl. Phys. **74**, 5546 (1993).
[11] F. L. Madarasz and F. Szmulowicz, Phys. Rev. B **24**, 4611 (1981).
[12] F. Szmulowicz, Phys. Rev. B **28**, 5943 (1983).
[13] J. M. Hinckley and J. Singh, Phys. Rev. B **41**, 2912 (1990).
[14] J. M. Hinckley and J. Singh, J. Appl. Phys. **76**, 4192 (1994).
[15] M. Dür, K. Unterrainer, and E. Gornik, Phys. Rev. B **49**, 13 991 (1994).
[16] J. E. Dijkstra and W. T. Wenckebach, J. Appl. Phys. **81**, 1259 (1997).
[17] R. Oberhuber, G. Zandler, and P. Vogl, Phys. Rev. B **58**, 9941 (1998).
[18] M. V. Fischetti and S. E. Laux, J. Appl. Phys. **80**, 2234 (1996).
[19] G. Sun and L. Friedman, Phys. Rev. B **53**, 3966 (1996).
[20] G. Sun, Y. Lu, L. Friedman, and R. A. Soref, Phys. Rev. B **57**, 6550 (1998).
[21] G. C. Crow and R. A. Abram, Semicond. Sci. Technol. **15**, 7 (2000).
[22] G. Sun, L. Friedman, and R. A. Soref, Phys. Rev. B **62**, 8114 (2000).
[23] J. D. Wiley, Solid State Commun. **8**, 1865 (1970).
[24] P. Harrison, *Quantum Wells, Wires and Dots: Theoretical and Computational Physics* (Wiley, Chichester, 1999).
[25] J. H. Marsh, Appl. Phys. Lett. **41**, 732 (1982).
[26] D. C. Look, D. K. Lorance, J. R. Sizelove, C. E. Stutz, K. R. Evans, and D. W. Whitson, J. Appl. Phys. **71**, 260 (1992).
[27] B. Laikhtman and R. A. Kiehl, Phys. Rev. B **47**, 10 515 (1993).
[28] K. Yeom, J. M. Hinckley, and J. Singh, J. Appl. Phys. **80**, 6773 (1996).
[29] P. J. Briggs, A. B. Walker, and D. C. Herbert, Semicond. Sci. Technol. **13**, 680 (1998).
[30] K. S. Yoon, G. B. Stringfellow, and R. J. Huber, J. Appl. Phys. **62**, 1931 (1987).
[31] M. J. Kearney and A. I. Horrell, Semicond. Sci. Technol. **13**, 174 (1998).
[32] J. A. Van Vechten and T. K. Bergstresser, Phys. Rev. B **1**, 3351 (1970).
[33] J. J. Tietjen and L. R. Weisberg, Appl. Phys. Lett. **7**, 261 (1965).
[34] J. W. Harrison and J. R. Hauser, Phys. Rev. B **13**, 5347 (1976).
[35] Y. Fu and M. Willander, J. Appl. Phys. **88**, 288 (2000).
[36] A. Yamada, N. Miyazono, and M. Konagai, Jpn. J. Appl. Phys. **38**, Pt.1, 2566 (1999).
[37] D. Girginoudi, A. Thanoilakis, N. Georgoulas, V. Kasabyan, and A. Christou, Superlattices Microstruct. **23**, 407 (1998).
[38] A. Kahan, M. Chi, and L. Friedman, J. Appl. Phys. **75**, 8012 (1994).
[39] C. G. Van de Walle and R. M. Martin, Phys. Rev. B **34**, 5621 (1986).